

# Optical Flow estimation with Event-based Cameras and Spiking Neural Networks

CUADRADO Javier<sup>\*1</sup>, RANÇON Ulysse<sup>1</sup>, COTTEREAU Benoit R.<sup>1,2</sup>,  
BARRANCO Francisco<sup>3</sup> and MASQUELIER Timothée<sup>1</sup>

<sup>1</sup>CerCo UMR 5549, CNRS – Université Toulouse III, Toulouse, France

<sup>2</sup>IPAL, CNRS IRL 2955, Singapore 138632

<sup>3</sup>Universidad de Granada, Granada, Spain

\*Corresponding Author

**Abstract**—Event-based cameras are raising interest within the computer vision community. These sensors operate with asynchronous pixels, emitting events, or “spikes”, when the luminance change at a given pixel since the last event surpasses a certain threshold. Thanks to their inherent qualities, such as their low power consumption, low latency and high dynamic range, they seem particularly tailored to applications with challenging temporal constraints and safety requirements. Event-based sensors are an excellent fit for Spiking Neural Networks (SNNs), since the coupling of an asynchronous sensor with neuromorphic hardware can yield real-time systems with minimal power requirements. In this work, we seek to develop one such system, using both event sensor data from the DSEC dataset and spiking neural networks to estimate optical flow for driving scenarios. We propose a U-Net-like SNN which, after supervised training, is able to make dense optical flow estimations. To do so, we encourage both minimal norm for the error vector and minimal angle between ground-truth and predicted flow, training our model with back-propagation using a surrogate gradient. In addition, the use of 3d convolutions allows us to capture the dynamic nature of the data by increasing the temporal receptive fields. Upsampling after each decoding stage ensures that each decoder’s output contributes to the final estimation. Thanks to separable convolutions, we have been able to develop a light model (when compared to competitors) that can nonetheless yield reasonably accurate optical flow estimates.

**Keywords**— optical flow, event vision, spiking neural networks, neuromorphic computing, edge AI

## I. INTRODUCTION

Computer vision has become a domain of major interest, both in research and in industry. Indeed, thanks to the development of new technologies, such as autonomous vehicles or self-operating machines, algorithms able to perceive the environment have proven to be key to achieving the desired level of performance. Among the numerous visual features these algorithms can estimate, optical flow (the pattern of apparent motion on the image plane due to relative displacements between an observer and his environment) remains one of paramount importance. Indeed, this magnitude is directly linked with depth and egomotion, and its rich, highly temporal information is precious for advanced computer vision applications, e.g. for obstacle detection and avoidance in autonomous driving systems. Given the severe safety constraints associated

with this kind of critical systems, accuracy and reliability are key to achieving successful models. However, achieving high levels of performance is not enough: the increasing concern about energy consumption motivates us to seek the most efficient model possible, all while retaining high-performance standards.

In the search of an energy-efficient way to estimate optical flow, we decided to focus our interest on event cameras. Unlike their regular, frame-based counterpart, this kind of sensor is composed of independent pixel processors, each firing asynchronous events when the variation of the detected luminance since the previous event reaches a given threshold, being this event of positive polarity if the brightness has increased, and of negative polarity otherwise. This behavior translates into enormous energy savings: whereas conventional frame-based cameras are forced by design to output a frame at a fixed frequency, event cameras do not trigger any events for static visual scenes. Furthermore, they show a higher dynamic range, which allows them to avoid problems such as image artifacts (e.g. saturation after leaving a tunnel while driving), and a lower latency than regular cameras, which makes them particularly suitable for challenging, highly dynamic tasks (event sensors do not suffer from motion blur, unlike their frame-based counterparts). Nevertheless, they can also be less expressive: event cameras only provide information regarding changes in luminance, and not about the luminance itself. Furthermore, most event cameras discard color information, although some devices exist with independent firing for RGB formation at each pixel, like the Color-DAVIS346 event camera used by [1] to generate their CED Dataset. Finally, event cameras usually have lower spatial resolution than regular cameras, although recent technological developments are bridging this gap (e.g. [2]).

In search of energy efficiency, the choice of the sensor is not enough: the optical flow prediction algorithm itself also has to be as efficient as possible to achieve our goal. That is why we have resorted to Spiking Neural Networks (SNNs) to develop our model. These bio-inspired algorithms, heavily inspired by the brain, consist of independent units (neurons), each of them with an inner membrane potential,

which can be excited or inhibited by pre-synaptic connections. When their inner potential reaches a certain, predefined firing threshold, one spike is sent to the post-synaptic neurons, and the membrane potential is reset. Since energy consumption on dedicated hardware is linked to spike activity, which is usually much sparser than standard analog neural networks activations, SNNs represent a more energy-efficient alternative. Moreover, in the absence of movement, no input events would be produced and fed to the network, which in turn would not trigger any spikes, and a zero-optical flow prediction would be achieved (which is indeed the desired behaviour, since no input events can only be achieved by a lack of relative motion).

Finally, optical flow being a highly temporal task, incorporating temporal context into our vision model is key to achieving acceptable levels of performance. Two alternatives exist: using stateful units within the network (e.g. LSTMs, GRUs or taking advantage of the intrinsic memory capabilities in the case of SNNs), or explicitly handling the temporal dependencies with convolutions over consecutive frames along a temporal axis. Exploiting spiking neuron inherent temporal dynamics has proven to be an extremely challenging task to achieve, and we have therefore opted for the second alternative.

To sum up, the main contributions of this article are:

- a novel angular loss, which can be used with standard MSE-like functions and which helps the network to learn an intrinsic spatial structure. To the best of our knowledge, we are the first to ever use such a function for optical flow estimation.
- 3d-encoding of input events over a temporal dimension, leading to increased optical flow estimation accuracy
- a hardware-friendly downsampling technique in the form of maximum pooling, that further improves the model’s accuracy
- a spiking neural network which can be implemented on neuromorphic chips, therefore taking advantage of their energy efficiency.

## II. RELATED WORK

Ever since their introduction, event cameras have been gaining ground within the computer vision community, and increasing efforts have been made to develop computer algorithms based on event data. As such, different datasets have emerged in order to solve different kinds of computer vision problems, like the DVS128 Gesture Dataset by [3] for gesture classification, or the EVIMO Dataset by [4] for motion segmentation and egomotion estimation. Despite this interest in event vision, the significant investment that event cameras represent for most research centers and companies has led to the development of event data simulators such as CARLA by [5], as well as algorithms to perform video-to-events conversion, like the model proposed in [6]. While lacking the intrinsic noise event data usually presents, these artificial data can nonetheless be used to efficiently pre-train computer vision neural networks, e.g. [7] pretraining their model for depth estimation on a synthetic set of event data.

Nonetheless, for real-world applications (e.g. gesture recognition, object detection, clustering, etc.), true event recordings are preferred because simulators are still lacking realistic event noise models. Concerning depth and/or optical flow regression, two datasets have currently established themselves as the go-to choices: the MVSEC Dataset by [8], and the DSEC Dataset by [9]. While all of these datasets have proven invaluable to develop event-based computer vision algorithms, there is still an enormous gap between event-based and image-based publicly available datasets, and many authors are still forced to develop their own. For example, [10] generated their own classification data from [11] to account for the additional “pedestrian” class.

Most models so far have either been standard Analog Neural Networks (ANNs) like [12], exploiting gated-recurrent units to achieve state-of-the-art accuracy on DSEC, or hybrid analog-spiking neural networks like [13], combining a spiking encoder with an additional analog encoder for grayscale images, followed by a standard ANN. Other models have tried to leverage the temporal context by feeding the network with not only the events themselves, but also information on event timestamps, like the EVFlowNet model presented in [14]. More recently, [15] showed temporal information to be a key in accurately estimating both optical flow and depth, achieving top results in the MVSEC and the DSEC datasets thanks to their implementation of non-spiking leaky integrators with learnable per-channel time constants. While all of these models do indeed achieve good levels of performance on their test sets, none of them manage to take advantage of the neuromorphic-friendly nature of event data, since analog blocks or additional non-spiking information prevent a deployment on neuromorphic chips.

More interesting to this work are spiking neural networks applied to event vision, be it for depth or for optical flow estimation. As far as optical flow is concerned, it is worth citing the works of [16], which achieves state-of-the-art levels of performance on the MVSEC Dataset with a fully spiking architecture. More recently, [17] showed that spiking neural networks can indeed compete with their analog counterparts in terms of accuracy, showing top results both in the MVSEC and in the DSEC Dataset. Finally, [18] achieve a remarkable accuracy on the MVSEC Dataset with a U-Net-like architecture and a self-supervised learning rule. However, all of these models are not implementable on neuromorphic hardware, since they either use upsampling techniques which are incompatible with the spiking nature of these devices (e.g. bilinear upsampling), or re-inject intermediate, lower-scale analog optical flow predictions, thereby violating the spiking constraint by introducing floating point values in an otherwise binary model. In addition, the choice of a self-supervised learning rule, usually linked to a photometric loss function presented in [19], means that optical flow estimations are only provided for pixels where events occurred, therefore creating non-dense flow maps. Looking at depth prediction though, we do find some interesting strategies for fully deployable neuromorphic models. Finally, authors in [20] presented in

their StereoSpike model a fully-spiking, hardware-friendly network achieving remarkable accuracy on the MVSEC Dataset, thanks to stateless spiking neurons that have greatly inspired our work.

### III. MATERIALS AND METHODS

#### A. Training Dataset

Our study focuses on driving scenes, and we chose the DSEC Dataset by [9] to train our model. Unlike previous state-of-the-art datasets, such as the Multi-Vehicle Stereo Event Camera (MVSEC) Dataset by [8], which provided different working scenarios (indoors/outdoors, day/night, and four possible vehicle configurations: pedestrian, motorbike, car and drone), the DSEC dataset only consists of driving scenario sequences. However, it provides higher-quality ground-truth labels, thanks to the finer processing of the LIDAR measurements. In addition, this dataset also includes masks for invalid pixels, i.e., pixels where the optical flow ground-truth is unknown. As such, our metrics have only been evaluated on the valid pixels. Furthermore, this dataset provides an open benchmark to submit the results, that we used to determine our test metrics and compare ourselves to other works.

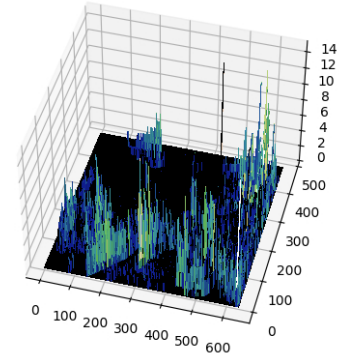
#### B. Input Event Representation

Event cameras produce an asynchronous event  $e_i$  when the luminance variation at a given pixel reaches a given threshold:

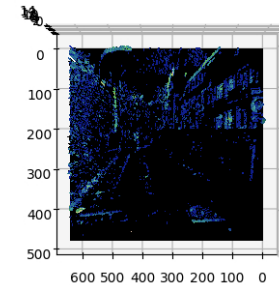
$$e_i = (x_i, y_i, t_i, p_i) \quad (1)$$

where  $(x_i, y_i)$  are the coordinates of the pixel emitting the event,  $t_i$  the event's timestamp, and  $p_i$  its polarity (+1 if luminance increases, and -1 otherwise). However, in order to perform our training, we are forced to work with a discrete time model, so a pre-processing of this event stream has to be made. We therefore transform the input event stream into a sequence of frames of a given length in milliseconds, that we call "input histograms". These frames consist of a two-channel ( $C = 2$ ) tensor of size  $(C, H, W)$ , where  $H$  and  $W$  represent the camera's resolution, i.e., the number of input pixels and their position in the camera. At each pixel, the first channel represents the number of positive input events that have been triggered in that particular pixel during the frame's duration, and the second channel represents the number of negative events. A representation of a one-channel input frame can be found in Figure 1. While not a binary representation, like the representation paradigm presented in [21], our choice is more expressive, since event counts account for pixel relative importance and therefore provide richer spatio-temporal information.

We acknowledge that this frame-based approach increases the model's latency, since event sensors can virtually function in continuous time. However, it is imposed by the nature of our training, and is a widespread technique for event-based learning (see [22] on event representations). Moreover, we can leverage the latency reduction by our frame duration choice: the input stream being a continuous sequence of events, we are free to cumulate them in windows of the desired duration.



(a) Perspective view



(b) Top view

Figure 1: Example of an input frame for 1 polarity. **(A)** Event cumulation at each pixel for a given time interval. **(B)** Top view of the event frame. We can see that events are heavily linked to contours (e.g. a zebra crossing on the bottom part, or the windows on a building on the right side), while regions with constant luminance (e.g. the road or the sky) do not trigger events.

#### C. Spiking Neuron Model

For our network, we chose a simple neuron model that can be easily implemented with open-source Python libraries, in addition to being much less computationally expensive than closer-to-nature neuron mathematical models. This model is the [23]. It was implemented using the Spikingjelly library, developed and maintained by [24], due to their full integration with the Pytorch library.

Our model is based on a stateless approach: the neuron's potential is reset after each forward pass. Indeed, the mathematical neuron model presented by McCulloch and Pitts consists of stateless neurons with Heaviside activation functions. This is equivalent to stateless integrate-and-fire neurons, i.e., stateless artificial neurons working as perfect integrators,

but which are reset at every time step. We therefore do not exploit the intrinsic memory capabilities of spiking neurons, but rather perform a binary encoding of the information. While this approach may seem counter-intuitive, it actually further reduces energy consumption, since the reset operation is usually less energy demanding than the neuronal leak, and no resources have to be allocated to long-term memory handling. Consequently, we do not need to model such phenomenon, and as a result our neuron model is more hardware friendly than its leaky counterpart. Temporal context is handled by 3d convolutions in the encoder stages of the model, as we explain in the following section.

#### D. Network Architecture

Our network is based on a U-Net-like architecture ([25]). Indeed, U-Net has established itself as a reference model when full-scale image predictions are required, i.e., predictions at roughly the same resolution as the input data. Our architecture is shown in Figure 2. After a first convolution stage which increases the number of channels to 32 without modifying the input tensor size, each encoder stage halves the tensor width and height while doubling the number of channels. Conversely, each decoder stage doubles the tensor width and height, and halves the number of channels.

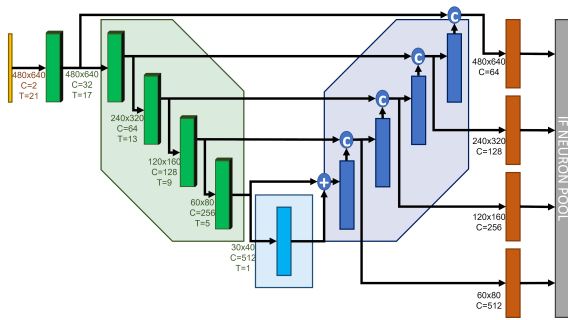


Figure 2: Our proposed network architecture. 3D Encoders ensure the incorporation of a temporal context within the model. Downsampling is performed via max. pooling to account for spatial spike activity. Each decoding stage is upsampled to contribute to the final network prediction.

In order to increase the network expressivity, each decoder stage plays a role in the final prediction. Each decoder output is upsampled into a full-scale, two-channel tensor (x- and y-components of the optical flow estimation). All of the outputs equally contribute to the network’s final estimation, which consists of the combination of successive coarse predictions. The loss function is evaluated after each update of the final neuron pool, thus forcing the network’s prediction to be close to the ground-truth as early as the first coarse update. This approach has been introduced in [20] and proved to be beneficial to increasing the overall accuracy.

The main features of our network are the following:

- Inspired by Temporal-Convolutional Networks, presented in [26] and [27], we use three-dimensional convolutions

for our data encoding. Consecutive input frames are combined by the temporal kernel via unpadded convolutions, decreasing the temporal dimension in size so it collapses to 1 when reaching the bottleneck. Afterwards, the network architecture is fully two-dimensional. By default, the temporal kernel size we use is 5, which leads to a temporal receptive field of  $21 \cdot 9ms = 189ms$  from the bottleneck and beyond.

- Skip connections between the encoder and the decoder consist of the last component of the temporal dimension at the corresponding encoding stage, since we believe the most recent event information to be the most relevant for optical flow estimation. We tested both sum and concatenate skip connections and found that concatenations led to the best estimations (these results are presented in subsection IV-B).
- Given the relative importance of the residual blocks in the total number of parameters, and in search of the lightest possible model, we also analyzed the effect of reducing the number of residuals on the network’s performance. We found that the best model only necessitated one residual, unlike other conventional U-Net-like architectures (e.g. [16]).
- Downsampling in the encoding stages is performed via maximum pooling, instead of traditional strided convolutions, to account for spikes within the kernel’s region, and not so much about individual spikes. This approach has proved to increase our model’s performance. To the best of our knowledge, it is the first time this technique is used in a U-Net-like spiking neural network for dense regression. In addition, [28] showed that this kind of downsampling strategy is supported by neuromorphic hardware.
- Since our final aim is to develop a model that could be implemented on a neuromorphic chip, the whole upsampling operation is performed via Nearest Neighbor upsampling, which preserves hardware friendliness.
- To further decrease the model’s weight, we used depth- and point-wise separable convolutions (see e.g. [29]) everywhere in the model. These convolutions do not only decrease the model’s number of parameters, but also reduce the model’s overfitting, therefore increasing its performance on unseen data.

It is important to specify that our approach is integer rather than binary-based, since some of our skip connections are additions instead of concatenations, and our bottleneck’s architecture is based on tensor sums. Nevertheless, our approach remains hardware-friendly, because:

- If the processing were asynchronous and event-driven, then the spikes arriving through the residual connection would typically arrive before the others. Thus, if there were two spikes, one from the residual and one from the normal connection, instead of doing an explicit ADD, both spikes could be fed through the same synapse, and each spike would cause an increment of  $w$  (instead of

adding the two spikes to get 2 and then multiplying by  $w$  to get the increment). Moreover, even if the spikes arrived synchronously, they would be processed sequentially using FIFO.

- Concatenation is equivalent to addition as a skip connection if the weights are duplicated and kept tight. Indeed, if there were two spikes, one from the residual and one from the "normal" connection, instead of doing  $2 \cdot w$ , the algorithm would perform  $w + w$ . Since the duplicated weights would be tight, the number of trainable parameters would be the same, and both operations would be equivalent.

### E. Supervised Learning Method

Our model was trained with supervised learning using the surrogate gradient descent, using a sigmoid function as our surrogate gradient model. The ground-truth optical flow values were those provided in the DSEC database. While traditional self-supervised methods restrict their optical flow processing to pixels where events occurred (e.g. [16], [14] or [17], to cite a few examples), our approach permits dense estimations (thanks to surrogate gradient learning). We trained our model on the valid pixels given by the dataset masks at each timestep.

Our loss function included two terms:

- A standard MSE-like loss between the value of the predicted flow and its corresponding ground truth, with the following formula:

$$L_{mod} = \frac{\sum^{N_{pixels}} \sqrt{\Delta_x^2 + \Delta_y^2}}{N_{pixels}}; \quad (2)$$

$$\Delta_i = pred_i - gt_i$$

The term  $N_{pixels}$  represents the number of valid pixels to be trained at each timestep.

- In addition to a penalization in modulus discrepancy between the vectors, we explicitly encourage the optical flow direction to be the same between the ground-truth and the prediction. This term has proven to be key to reduce noise in optical flow predictions, since pixels with low optical flow values consistently yield small modulus loss values regardless of their direction. We used the following formula:

$$L_{ang} = \frac{\sum^{N_{pixels}} \text{acos}(c\theta)}{N_{pixels}}; \quad (3)$$

$$c\theta = \frac{\vec{gt} \cdot \vec{pred} + \epsilon}{|\vec{gt}| \cdot |\vec{pred}| + \epsilon}$$

where  $c\theta$  is the cosine of the error angle between the predicted and the ground-truth flow, and epsilon is a small parameter ( $\epsilon = 10^{-7}$ ) to ensure that no errors are found within the code during execution. Furthermore, the values of  $c\theta$  are clamped between  $(-1 + \epsilon, 1 - \epsilon)$  for the same reason.

The final loss function used to train the model is:

$$L = \lambda_{mod} \cdot L_{mod} + \lambda_{ang} \cdot L_{ang} \quad (4)$$

From preliminary tests, we found that  $\lambda_{mod} = \lambda_{ang} = 1$  yields good results, and we therefore decided to use these values.

As explained in subsection III-D (Network Architecture), each decoder's output plays a role in the final optical flow estimation. As such, and in order to encourage accuracy since the first decoder's upsampling, the loss function is evaluated for each consecutive contribution to the final pool. After each upsampling of the decoder's output, the inner potentials of an IF layer are updated, and the loss is evaluated on those potentials equivalent to summing the spikes out of each decoder stage weighted by the corresponding intermediary prediction layer.

Finally, in order to perform the back-propagation in our supervised training method, we resorted to surrogate gradient learning, introduced in [30], and already implemented in the SpikingJelly library [24].

### F. Training Details

All of our calculations were performed on either NVIDIA A40 GPUs, or in Tesla V100-SXM2-16GB GPUs belonging to the French regional public supercomputer CALMIP, owned by the Occitanie region.

Trainings were realized with a batch size of 1, since it is the optimal value we have found for our task. Although unconventional, this result is in line with the one found in [20], where a batch size of one was found optimal for depth regression from event data using stateless spiking neurons. We used an exponential learning rate scheduler, and have implemented random horizontal flip as a data augmentation technique to improve performance. Furthermore, thanks to our stateless approach, we were able to train our network with shuffled samples, instead of being forced to use the input frames sequentially.

## IV. RESULTS

We divided our dataset into a train and a validation split, and our performance levels are reported with regard to the validation set. The exact sequences used in each split can be found in the supplementary materials. Nevertheless, we resort to the official DSEC benchmark to compare ourselves to the state-of-the-art, since it represents an objective, third-party test set. We now proceed to present the results we obtained in our studies. Due to the number of tests that we have run, all of the corresponding plots are provided in the Supplementary Materials.

### A. Finding the optimal kernel size

Convolutional neural networks have regained the interest of the deep learning community during the past few years, thanks to their ability to capture spatial relations within their kernel. Recently, increased kernel sizes have been replacing the traditional 3x3 formula, with examples as relevant as [31], which uses 7x7 kernels. [32] presents a method to scale up the kernel size to 31x31, and [33] goes even further and proposes to go up to 51x51 for the spatial kernel size, although both of these methods rely on sparsity and re-parametrization to

achieve their goal. Starting from a naive U-Net like model, we started our research by trying to optimize our spatial kernel size. In the end, our results do match those presented in [32], showing that 7x7 kernels are optimal. Indeed, further increasing the kernel size makes computational time explode, while accuracy plateaus. We therefore decided to adopt a 7x7 kernel in the spatial dimension for our model.

Next, we optimized the temporal kernel size, directly linked with the number of frames that we input to our model. Since we want the temporal dimension to collapse to one in the bottleneck thanks to unstrided convolutions in the temporal dimension, a larger kernel size naturally requires a greater number of frames, and therefore a heavier model. Nonetheless, it also takes into account a longer temporal context, which may be beneficial for the network’s accuracy. As such, we tested our simple model for temporal kernel sizes of 3 (11 input frames), 5 (21 input frames) and 7 (31 input frames). Our results show that increasing the kernel size up to 5 does indeed boost the model’s accuracy, but going beyond this size does not translate into an accuracy improvement. Thus, a temporal kernel size of 5 was chosen for the 3d convolutions in our model.

### B. Finding the best network architecture

In order to find the best network architecture, we evaluated two possible options:

- We compared sum vs. concatenate skip connections, since concatenate skip connections are easier to implement in neuromorphic hardware, but slightly increase the number of parameters in the network.
- Seeking to develop a model as light as possible, we also characterized the effect of the number of residuals in the network’s bottleneck on the model’s performance.

After training each of the models for 35 epochs, we found the best model to be the 1-residual network with concatenate skip connections, which amounts to a total of 1.22 million of parameters and leads to an accuracy of 1.1 pixels/second of average end-point error on our validation dataset, using 9ms frames as an input in all cases. The results regarding the architecture optimization have been summarized in Table I.

### C. Optimizing the frame duration

Next, we focused our attention on the optimal frame duration to accurately estimate optical flow, i.e., the total temporal context the network processes when making a prediction. This parameter is directly linked with the latency the model can achieve, since optical flow estimations are only produced at the end of each frame (provided that the input tensors are treated as a sliding window, where only the last  $N=21$  frames are considered).

We trained the network with frames of 4.5 ms, 9 ms and 18 ms respectively. Our results show that the optimal frame duration was 9 ms, followed by 18 ms, and finally we get the worst performance for frames of 4.5 ms. While it may seem counter-intuitive as a results, since 4.5 ms frames

contain a finer representation of the event sequence, we believe this phenomenon is caused by the lack of overall temporal context. Indeed, by using short frames, the network is unable to extract longer-term dependencies, and therefore to accurately predict optical flow. That is also why we believe that 18ms frames, while coarser, do manage to better capture these long term dependencies, and therefore provide a more accurate estimation. These results, as well as all of the successive optimization studies we have performed, can be found on Table II.

### D. Comparison with the state-of-the-art

We trained our best architecture on the whole DSEC dataset for a total of 100 epochs. We evaluated our model on the official test set provided by DSEC. Results are shown on Table III. In order to provide a fair comparison, we only included results on the official benchmark, and not those reported on custom validation sets. While still far from the best models, we demonstrate the power of spiking neural networks when applied to dense regression in computer vision, achieving good levels of performance with a fraction of parameters when compared to other models.

We also provide some of our model’s results on the validation set, which can be found in Figure 3. These pictures show that, even if the network was not explicitly trained to distinguish image contours (since it was only trained on a selection of valid pixels at each timestep), it is nonetheless capable of extracting structural information within the scene and generalizing it, as illustrated in the rightmost images (unmasked predictions) for the given examples. These results demonstrate the model’s general comprehension of the visual scene, and we believe represent a solid understanding of the pattern of motion.

### E. Ablation studies

Several ablation studies have been performed on our best model to further demonstrate our claims, and we have gathered our conclusions in the following paragraphs. Plots containing all of these results can be found in the Supplementary Materials.

1) *Pooling vs. Convolutional Downsampling*: Our results show that using maximum pooling instead of strided convolutions is an efficient technique to downsample spiking data. We believe that the reason behind this behavior is that pooling is a way of densifying the tensors without changing their spiking nature.

2) *3d vs. 2d Encoding*: We also compared our baseline 3d model with an equivalent 2d model, where the 21 input frames have been fed to the network concatenated along the channel dimension, so that both models have the same temporal context. We found out that fully 2-dimensional models lead to decreased performance. We believe this is due to the fact that, by using 2d convolutions, all the temporal information is directly mixed during the first convolution stage, therefore hindering the network from finding long-term dependencies.

3) *Loss function*: We also analyzed the influence of the loss function on the final results obtained. We compared our proposed loss model to two single-term losses:

- One model with only the norm of the error vector, but without the angular loss term
- One loss function with only a relative loss term:

$$L_{relative} = \frac{1}{N_{pixels}} \frac{\sum^{N_{pixels}} \sqrt{\Delta_x^2 + \Delta_y^2}}{\sqrt{gt_x^2 + gt_y^2 + \epsilon}}; \quad (5)$$

$$\Delta_i = pred_i - gt_i$$

This model penalizes deviations in the prediction relative to the ground truth’s norm, and should therefore be able to implicitly impose a restriction on angular accuracy.

Our results show that naively limiting the error’s norm is not enough to achieve competitive results, and neither is limiting the relative error. Indeed, by introducing a more aggressive term in the loss function, we managed to force the network into implicitly learning the optical flow’s structure, and therefore achieve better accuracy.

It is surprising that the network with the two losses reaches a lower  $L_{mod}$  than the network with  $L_{mod}$  only. This shows that the second network gets trapped in a local minima and that adding the  $L_{ang}$  loss helps to get out of it.

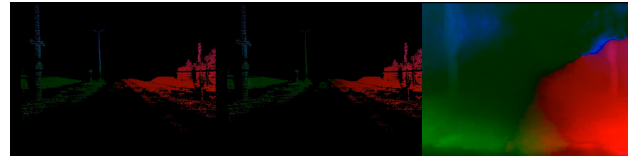
4) *Effect of combining polarities on performance*: Our next study on input representation has consisted in combining polarities into a single channel before feeding them to the model. Polarities being closely linked to phenomena like color or texture, we wish to study their influence on the final performance levels. Indeed, if we imagine a grey background with a black shape and a white shape following the same track, we would obtain opposite polarity fronts, while the optical flow pattern would be the same. We have therefore analyzed if polarities can be simply combined into a total per-pixel event count.

However, our results show that keeping separate channels for each polarities is beneficial for the network’s performance. We believe this result is linked to the different dynamics linked to each of the polarities, since different thresholds lead to different behaviour for luminance increments or decrements.

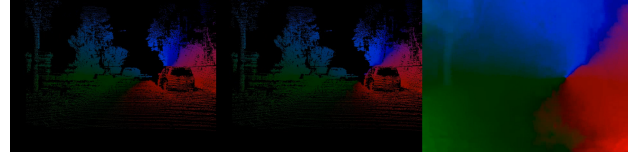
5) *Skip connections in the bottleneck*: Our final ablation study targeted the very first skip connection, i.e., connecting the last encoder with the first decoder. Having always kept it as a sum (slightly redundant, given the residual block architecture) because of the high number of channels, we have also tested transforming it into a cat skip connection. However, we found out that it decreases the network’s performance while also increasing the number of parameters. We therefore decided to keep it as a sum for all of the architectures.

## V. DISCUSSION

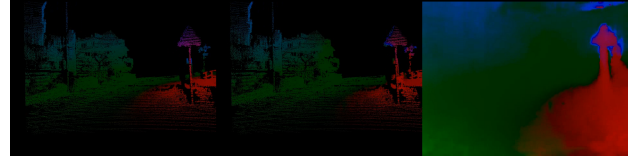
To sum up, we present a hardware-friendly, lightweight spiking model able to accurately estimate optical flow from event-based data collected by neuromorphic vision sensors. We propose an efficient temporal coding in the form of



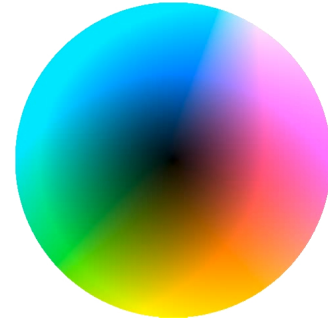
(a) Optical flow discontinuities due to vertical artifacts within the visual scene.



(b) The silhouette of the leftmost tree can be perceived on the unmasked optical flow map.



(c) Traffic signs clearly distinguishable on the right side



(d) Optic Flow Encoding

Figure 3: Example predictions of our best architecture on our validation set. For every picture, the leftmost image is the ground-truth, the middle image shows our masked estimation (only on valid pixels), and the rightmost image represents the unmasked estimation. Subfigure 3d represents the chosen colormap for optical flow representation: Optical flow is encoded as an Lab image, where the luminance channel represents the absolute magnitude of the flow, and the a and b channels the different directions.

3d convolutions in the encoder that increases the temporal receptive field of the deepest stages of the network. We also introduce a novel angular loss function that, in conjunction with a standard MSE-like loss, manages to boost performance by forcing the algorithm to learn the implicit spatial structure. We use maximum pooling as our downsampling strategy, thus densifying the tensors in a neuromorphic-friendly fashion. Moreover, the successive contributions of decoder outputs to the final prediction increase the network’s expressivity, and allow us to achieve competitive results without resorting to intermediate prediction re-injections. Consequently, our model can be implemented in neuromorphic hardware, thus resulting in an extremely energy efficient model that can still achieve

Model	Mod Loss	Angular Loss	Num. Params (M)
1 residual + sum skip connections	1.18	0.101	1.1
<b>1 residual + cat skip connections</b>	<b>1.10</b>	<b>0.094</b>	<b>1.2</b>
2 residual + sum skip connections	1.15	0.097	1.7
2 residual + cat skip connections	1.16	0.109	1.8

Table I: Performance comparison for the different proposed architectures. All of the models have been trained for 35 epochs, using 21 input frames of 9ms each.

Model	Modifications	Mod Loss	Angular Loss
<b>1 res + cat</b>	-	<b>1.10</b>	<b>0.094</b>
2 res + sum	-	1.15	0.097
1 res + cat	4.5ms frames	1.41	0.129
2 res + sum	4.5ms frames	1.42	0.130
1 res + cat	18ms frames	1.19	<u>0.087</u>
2 res + sum	18ms frames	1.32	0.102
1 res + cat	combined polarities	1.14	0.092
2 res + sum	combined polarities	1.31	0.112

Table II: Performance comparison. The two best models have been tested for different slight modifications of the architecture, keeping the number of parameters mostly unchanged.

Model	AEE (px/s)	AAE (deg)	Num. Params (M)
E-RAF [12]	<b>0.79</b>	<b>2.9</b>	5.3
Ours	1.71	6.3	<b>1.2</b>
MultiCM [34]	3.47	14.0	-

Table III: Comparison with the state-of-the art, obtained from <https://dsec.ifi.uzh.ch/uzh/dsec-flow-optical-flow-benchmark/>

accurate predictions.

We believe our results contribute to promote spiking neural networks as energy-efficient, real-world alternatives to traditional computer vision systems, based on frame-based video treatment and/or complex sensor data. However, we acknowledge that work has yet to be done, since a lot of the intrinsic potential of SNNs, namely their inherent memory handling capabilities, has not been fully exploited in this study. Moreover, the convergence of our experiments to an optimal batch size of 1, while having indeed improved our model’s performance, greatly hinders the training speed, since strategies such as data parallelization cannot be employed. We therefore believe that these results can be further improved, e.g. using techniques such as weight averaging or network pre-training.

Future research lines should focus on further combining different techniques in order to boost performance even further. For instance, exploiting the intrinsic memory of spiking neurons is indeed a potentially useful approach, but the increased computational power linked to unrolling a stateful computational graph makes the task challenging. Moreover,

sensor fusion can also be explored as an alternative to boost performance, especially since most event cameras often also provide black and white images. This approach could increase the network’s latency, as well as making neuromorphic implementation challenging. Furthermore, while temporal dependencies have been imposed a priori in our model, they could also be natively learnt by the network. The works of [35] present a way of increasing kernel sizes without an increment in network parameters, capable of achieving state-of-the-art performances. While only applied so far for 1- and 2-dimensional convolutions, their method could easily be adapted to our 3d approach.

Moreover, publicly available datasets usually lack challenging conditions, such as crossing pedestrians or vehicles, which can limit the network’s generalization capabilities. While we believe that our proposed model is capable of understanding such situations (see Subfigure 3c, where traffic signals are easily recognizable), it would be desirable to train on more challenging scenarios.

#### AUTHOR CONTRIBUTIONS

All authors conceptualized the study and analyzed the results. JC designed, programmed, and ran the simulations. JC wrote the main core of the article. All the authors provided comments to achieve the final version of the paper.

#### FUNDING

This research was supported in part by the Agence Nationale de la Recherche under Grant ANR-20-CE23-0004-04 “DeepSee”, by the Spanish National Grant PID2019-109434RA-I00/ SRA (State Research Agency /10.13039/501100011033), by the Program DesCartes and by the National Research Foundation, Prime Minister’s Office, Singapore under its Campus for Research Excellence and Technological Enterprise (CREATE) Program.

#### ACKNOWLEDGMENTS

This work was granted access to the HPC resources of CALMIP supercomputing center under the allocation 2016-p22020.

The authors would also express their gratitude to the CerCo’s NeuroAI team, and specially to Mr. Khalfouli-Hassani, for their constant support and insightful feedback. We would also like to thank Mr. Fang, developer of the SpikingJelly library, for the constant support he has provided during the whole timespan of this study.



## DATA AVAILABILITY STATEMENT

The DSEC Dataset, chosen to develop our models, can be found on the “DSEC Dataset” website (<https://dsec.ifi.uzh.ch/>). In addition, all of our codes can be found on the following GitHub repository: [https://github.com/J-Cuadrado/OE\\_EV\\_SNN](https://github.com/J-Cuadrado/OE_EV_SNN)

## REFERENCES

- [1] C. Scheerlinck, H. Rebecq, T. Stoffregen, N. Barnes, R. Mahony, and D. Scaramuzza, “Ced: Color event camera dataset,” pp. 0–0, 2019.
- [2] PROPHESSEE, “Metavision packaged sensor,” <https://www.prophesee.ai/event-based-sensor-packaged/>, 2021, accessed: 2023-01-24.
- [3] A. Amir, B. Taba, D. Berg, T. Melano, J. McKinstry, C. Di Nolfo, T. Nayak, A. Andreopoulos, G. Garreau, M. Mendoza *et al.*, “A low power, fully event-based gesture recognition system,” in *Proceedings of the IEEE conference on computer vision and pattern recognition*, 2017, pp. 7243–7252.
- [4] L. Burner, A. Mitrokhin, C. Fermüller, and Y. Aloimonos, “Evim2: An event camera dataset for motion segmentation, optical flow, structure from motion, and visual inertial odometry in indoor scenes with monocular or stereo algorithms,” *arXiv preprint arXiv:2205.03467*, 2022.
- [5] A. Dosovitskiy, G. Ros, F. Codevilla, A. Lopez, and V. Koltun, “CARLA: An open urban driving simulator,” in *Proceedings of the 1st Annual Conference on Robot Learning*, 2017, pp. 1–16.
- [6] D. Gehrig, M. Gehrig, J. Hidalgo-Carrió, and D. Scaramuzza, “Video to events: Recycling video datasets for event cameras,” in *Proceedings of the IEEE/CVF Conference on Computer Vision and Pattern Recognition*, 2020, pp. 3586–3595.
- [7] J. Hidalgo-Carrió, D. Gehrig, and D. Scaramuzza, “Learning monocular dense depth from events,” in *2020 International Conference on 3D Vision (3DV)*, 2020, pp. 534–542.
- [8] A. Z. Zhu, D. Thakur, T. Özaskan, B. Pfrommer, V. Kumar, and K. Daniilidis, “The multivehicle stereo event camera dataset: An event camera dataset for 3d perception,” pp. 2032–2039, 2018.
- [9] M. Gehrig, W. Aarents, D. Gehrig, and D. Scaramuzza, “Dsec: A stereo event camera dataset for driving scenarios,” 2021.
- [10] L. Cordone, B. Miramond, and P. Thierion, “Object detection with spiking neural networks on automotive event data,” in *2022 International Joint Conference on Neural Networks (IJCNN)*. IEEE, 2022, pp. 1–8.
- [11] P. de Tournemire, D. Nitti, E. Perot, D. Migliore, and A. Sironi, “A large scale event-based detection dataset for automotive,” 2020. [Online]. Available: <https://arxiv.org/abs/2001.08499>
- [12] M. Gehrig, M. Millhäusler, D. Gehrig, and D. Scaramuzza, “E-raft: Dense optical flow from event cameras,” in *International Conference on 3D Vision (3DV)*, 2021.
- [13] C. Lee, A. K. Kosta, and K. Roy, “Fusion-flownet: Energy-efficient optical flow estimation using sensor fusion and deep fused spiking-analog network architectures,” in *2022 International Conference on Robotics and Automation (ICRA)*, 2022, pp. 6504–6510.
- [14] A. Z. Zhu, L. Yuan, K. Chaney, and K. Daniilidis, “Ev-flownet: Self-supervised optical flow estimation for event-based cameras,” *arXiv preprint arXiv:1802.06898*, 2018.
- [15] K. Zhang, K. Che, J. Zhang, J. Cheng, Z. Zhang, Q. Guo, and L. Leng, “Discrete time convolution for fast event-based stereo,” in *Proceedings of the IEEE/CVF Conference on Computer Vision and Pattern Recognition (CVPR)*, June 2022, pp. 8676–8686.
- [16] J. Hagenaars, F. Paredes-Vallés, and G. De Croon, “Self-supervised learning of event-based optical flow with spiking neural networks,” *Advances in Neural Information Processing Systems*, vol. 34, pp. 7167–7179, 2021.
- [17] A. K. Kosta and K. Roy, “Adaptive-spikenet: Event-based optical flow estimation using spiking neural networks with learnable neuronal dynamics,” *arXiv preprint arXiv:2209.11741*, 2022.
- [18] Y. Zhang, H. Lv, Y. Zhao, Y. Feng, H. Liu, and G. Bi, “Event-based optical flow estimation with spatio-temporal backpropagation trained spiking neural network,” *Micromachines*, vol. 14, no. 1, p. 203, 2023.
- [19] J. J. Yu, A. W. Harley, and K. G. Derpanis, “Back to basics: Unsupervised learning of optical flow via brightness constancy and motion smoothness,” 2016. [Online]. Available: <https://arxiv.org/abs/1608.05842>
- [20] U. Rançon, J. Cuadrado-Anibarro, B. R. Cottreau, and T. Masquelier, “Stereospike: Depth learning with a spiking neural network,” *IEEE Access*, vol. 10, pp. 127 428–127 439, 2022.
- [21] L. Cordone, B. Miramond, and S. Ferrante, “Learning from event cameras with sparse spiking convolutional neural networks,” in *2021 International Joint Conference on Neural Networks (IJCNN)*, 2021, pp. 1–8.
- [22] G. Gallego, T. Delbruck, G. Orchard, C. Bartolozzi, B. Taba, A. Censi, S. Leutenegger, A. J. Davison, J. Conradt, K. Daniilidis, and D. Scaramuzza, “Event-based vision: A survey,” *IEEE Transactions on Pattern Analysis and Machine Intelligence*, vol. 44, no. 1, pp. 154–180, Jan 2022. [Online]. Available: <https://doi.org/10.1109%2Ftpami.2020.3008413>
- [23] W. S. McCulloch and W. Pitts, “A logical calculus of the ideas immanent in nervous activity,” *The bulletin of mathematical biophysics*, vol. 5, no. 4, pp. 115–133, 1943.
- [24] W. Fang, Y. Chen, J. Ding, D. Chen, Z. Yu, H. Zhou, T. Masquelier, Y. Tian, and other contributors, “Spikingjelly,” <https://github.com/fangwei123456/spikingjelly>, 2020, accessed: 2023-01-11.
- [25] O. Ronneberger, P. Fischer, and T. Brox, “U-net: Convolutional networks for biomedical image segmentation,” in *International Conference on Medical image computing and computer-assisted intervention*. Springer, 2015, pp. 234–241.
- [26] C. Lea, R. Vidal, A. Reiter, and G. D. Hager, “Temporal convolutional networks: A unified approach to action segmentation,” in *European conference on computer vision*. Springer, 2016, pp. 47–54.
- [27] C. Lea, M. D. Flynn, R. Vidal, A. Reiter, and G. D. Hager, “Temporal convolutional networks for action segmentation and detection,” in *proceedings of the IEEE Conference on Computer Vision and Pattern Recognition*, 2017, pp. 156–165.
- [28] R. Gaurav, B. Tripp, and A. Narayan, “Spiking approximations of the maxpooling operation in deep snns,” *arXiv preprint arXiv:2205.07076*, 2022.
- [29] F. Chollet, “Xception: Deep learning with depthwise separable convolutions,” in *Proceedings of the IEEE conference on computer vision and pattern recognition*, 2017, pp. 1251–1258.
- [30] E. O. Neftci, H. Mostafa, and F. Zenke, “Surrogate gradient learning in spiking neural networks: Bringing the power of gradient-based optimization to spiking neural networks,” *IEEE Signal Processing Magazine*, vol. 36, no. 6, pp. 51–63, 2019.
- [31] Z. Liu, H. Mao, C.-Y. Wu, C. Feichtenhofer, T. Darrell, and S. Xie, “A convnet for the 2020s,” in *Proceedings of the IEEE/CVF Conference on Computer Vision and Pattern Recognition*, 2022, pp. 11 976–11 986.
- [32] X. Ding, X. Zhang, J. Han, and G. Ding, “Scaling up your kernels to 31x31: Revisiting large kernel design in cnns,” in *Proceedings of the IEEE/CVF Conference on Computer Vision and Pattern Recognition (CVPR)*, June 2022, pp. 11 963–11 975.
- [33] S. Liu, T. Chen, X. Chen, X. Chen, Q. Xiao, B. Wu, M. Pechenizkiy, D. Mocanu, and Z. Wang, “More convnets in the 2020s: Scaling up kernels beyond 51x51 using sparsity,” *arXiv preprint arXiv:2207.03620*, 2022.
- [34] S. Shiba, Y. Aoki, and G. Gallego, “Secrets of event-based optical flow,” in *Computer Vision—ECCV 2022: 17th European Conference, Tel Aviv, Israel, October 23–27, 2022, Proceedings, Part XVIII*. Springer, 2022, pp. 628–645.
- [35] I. Khalfaoui-Hassani, T. Pellegrini, and T. Masquelier, “Dilated convolution with learnable spacings,” 2021. [Online]. Available: <https://arxiv.org/abs/2112.03740>

# Supplementary Materials

## 1 Train and validation split

Here is the sequence division we have done for our train and validation split:

- Trainin split:
  - zurich\_city\_01\_a
  - zurich\_city\_02\_a
  - zurich\_city\_02\_c
  - zurich\_city\_01\_e
  - zurich\_city\_05\_a
  - zurich\_city\_05\_b
  - zurich\_city\_06\_a
  - zurich\_city\_07\_a
  - zurich\_city\_09\_a
  - zurich\_city\_10\_a
  - zurich\_city\_10\_b
  - zurich\_city\_11\_a
  - zurich\_city\_11\_c
- Validation split:
  - thun\_00\_a
  - zurich\_city\_02\_d
  - zurich\_city\_03\_a
  - zurich\_city\_08\_a
  - zurich\_city\_11\_b

The data split has been performed in order to ensure around 75% of the available data being used during training, while the remaining 25% was used in evaluation.

## 2 Result Plots

Here are the plots containing the results of our trainings, evaluated on our validation split. The naming convention for each run is the following:

- mono- : all of our results have been obtained using event data from the left camera
- k5 : temporal kernel size of 5
- p2 : pooling kernel size of 2
- 1res or 2res : number of residuals
- Xms : frame duration
- 1pol or 2pol : whether or not polarities were combined as a single channel
- sum or cat : nature of the skip connections
- wDA : the training was done with data augmentation (random horizontal flip)
- lr2e-4 : initial learning rate
- Further notes concerning the training (e.g. modification of the loss function, architectural changes, ...)

## 3 Supplementary Tables and Figures

### 3.1 Results

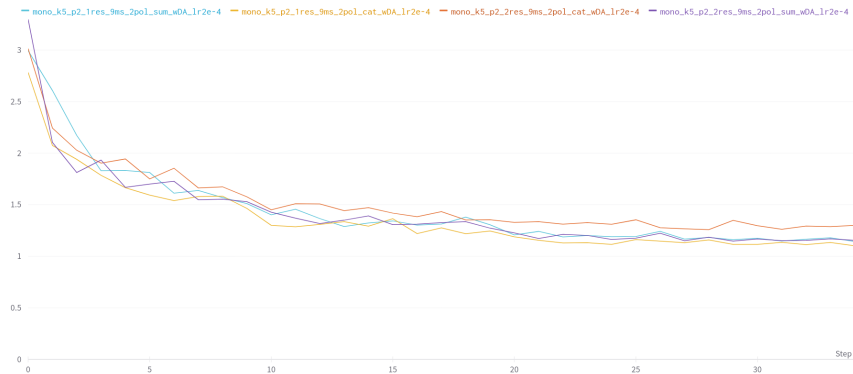


Figure 1: Architecture optimization (1 vs. 2 residuals, and ADD vs. CAT skip connections).

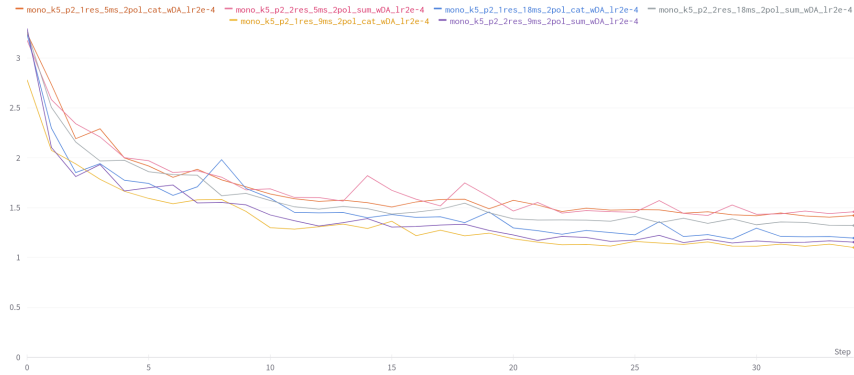


Figure 2: Frame duration optimization: 4.5ms, 9ms and 18 ms.

All sequence averages	interlaken_00_b	interlaken_01_a	thun_01_a	thun_01_b	zurich_city_12_a	zurich_city_14_c	zurich_city_15_a
<b>1PE</b>	<b>1PE</b>	<b>1PE</b>	<b>1PE</b>	<b>1PE</b>	<b>1PE</b>	<b>1PE</b>	<b>1PE</b>
53.671	64.72	56.265	51.414	55.15	49.698	54.037	44.138
<b>2PE</b>	<b>2PE</b>	<b>2PE</b>	<b>2PE</b>	<b>2PE</b>	<b>2PE</b>	<b>2PE</b>	<b>2PE</b>
20.238	36.43	25.856	14.785	16.668	12.662	21.65	11.75
<b>3PE</b>	<b>3PE</b>	<b>3PE</b>	<b>3PE</b>	<b>3PE</b>	<b>3PE</b>	<b>3PE</b>	<b>3PE</b>
10.308	23.514	14.925	5.929	6.378	3.852	9.956	4.892
<b>EPE</b>	<b>EPE</b>	<b>EPE</b>	<b>EPE</b>	<b>EPE</b>	<b>EPE</b>	<b>EPE</b>	<b>EPE</b>
1.707	3.07	1.902	1.361	1.406	1.241	1.576	1.241
<b>AE</b>	<b>AE</b>	<b>AE</b>	<b>AE</b>	<b>AE</b>	<b>AE</b>	<b>AE</b>	<b>AE</b>
6.338	4.678	5.321	6.365	6.17	9.218	6.686	6.293

Figure 3: Achieved accuracy on the DSEC Official Test Set (<https://dsec.ifi.uzh.ch/>): overall metrics and per-sequence performance.

### 3.2 Ablation Studies



Figure 4: Accuracy comparison between strided convolutions (orange) and strided maximum pooling (yellow) as downsampling strategies.



Figure 5: Accuracy comparison between our proposed 3d-encoder architecture (yellow) and an equivalent fully 2-dimensional architecture (purple).



Figure 6: Influence of the angular term in the loss function on the achieved accuracy.

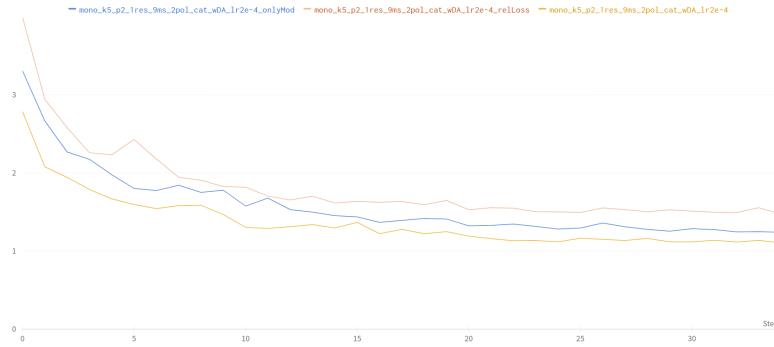


Figure 7: Influence of the loss function on the achieved accuracy (validation set): best loss model (yellow), norm of the error vector (blue) and relative error (light orange).



Figure 8: Effect of combining the polarities in a single channel on the final validation performance.

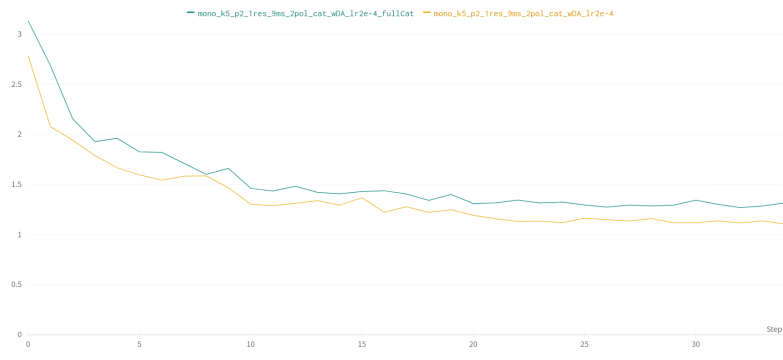


Figure 9: Influence of the first skip connection (last encoder with first decoder) on the model’s performance: the yellow curve represents our base model, whereas the blue curve represents a CAT skip connection between linking the encoder’s output and the decoder’s input.